Int. J. Electrochem. Sci., 12 **(2017)** 7205 – 7215, doi: 10.20964/2017.08.60

International Journal of
ELECTROCHEMICAL
SCIENCE
www.electrochemsci.org

Role of HCO_3^- and Cl^- in the Pitting of 20CrMo Steel in simulated oil field environment

Bingying Wang[*], *Ting Xin, Zhiwei Gao*

School of Mechanical and Electrical Engineering, China University of Petroleum, Qingdao 266580, China
[*]E-mail: tdwby2004@126.com

Received: 3 May 2017 / *Accepted:* 17 June 2017 / *Published:* 12 July 2017

In this study, the effects of HCO_3^- and Cl^- concentrations on the pitting behavior of 20CrMo steel were investigated by potential polarization curve, electrochemical impedance spectroscopy and Mott-Schottky measurements. In addition, the concentrations of HCO_3^- and Cl^- in a simulated oil field environment were varied to investigate the interactions between HCO_3^- and Cl^-. The results indicated that with increasing HCO_3^- concentration, the passivation of HCO_3^- is enhanced, leading to the increase in the corrosion and pitting potentials and decrease in the number of defects in the passivation film as well as the corrosion current. With increasing Cl^- concentration, the erosion became severe, resulting in the loosening and breaking of the passivation film as well as the easy formation of holes. The $[Cl^-]/[HCO_3^-]$ ratio exhibited a concentration threshold. The passivation of HCO_3^- played a dominant role below the critical value; the erosion effect of Cl^- is main role above the critical value and 20CrMo steel occurs dissolution.

Keywords: 20CrMo steel; pitting corrosion; polarization curve; passivation film

1. INTRODUCTION

As the majority of the oil fields have entered the extra-high water period, several corrosive media are present in the fluid, and the degree of mineralization is high. The localized corrosion of sucker rods has attracted considerable attraction. The high concentrations of HCO_3^- and Cl^- in the environment, main affect corrosion.

Li et al. [1] and Du et al. [2] have independently reported that the HCO_3^- in the environment plays a significant role in the corrosion behavior of pipeline steels. Li et al. [3] have investigated the corrosion behavior of X80 steel in HCO_3^- solution. The contact of pipeline steel with high pH soil, leads to the formation of a passivation film. Because of the presence of HCO_3^- in the soil, the effect of

HCO_3^- on the corrosion of the pipeline steel is more complicated [4]. HCO_3^- might form an oxide film with Fe^{2+} to prevent the anodic dissolution. On the contrary, HCO_3^- might break the corrosion product film, here by initiating pitting and stress corrosion cracking [5]. Hamadou et al. [6] have reported the correlation between the type of semiconductor and the pitting behavior of the passive film on carbon steel at different potentials.

The strong erosion by Cl^- can cause the localized rupture of the passivation film, leading to the initiation of pitting [7]. P. Marcus et al. [8] have reported that pitting result from the competitive adsorption of Cl^- and OH^- in solution. Cheng et al. [9] have pointed out that Cl^- leads to the occurrence of pitting as a result of the increase in the probability of localized rupture of the passivation film rather than the preventing of surface repassivation. Above a certain chloride threshold concentration, the passivation film on the reinforcing steel breaks down, inducing the pitting corrosion of steel [10-13]. Zuo Y et al. [14,15] have reported that Cl^- exerts a similar effect on the metastable pitting potential(Em) and pitting potential(Eb) values of carbon steel and stainless steel.

When the $[Cl^-]/[OH^-]$ ratio exceeds the threshold, the breakdown and repassivation of the passivation film at the local active site on rebars probably cause fluctuations in the potential and current [16]. The localized corrosion readily occurs in case the $[Cl^-]/[OH^-]$ ratio exceeds 0.2–2 [17,18].

In the previous investigation, although several studies have been conducted to elucidate the pitting behavior of carbon steel in single- and double-ion systems and the relationship between the $[Cl^-]/[OH^-]$ ratio and electrochemical corrosion, few studies have focused on the corrosion behavior of 20CrMo steel in simulated oil field environment. The corrosion mechanism and the interactions between HCO_3^- and Cl^- need to be investigated further. In this study, the effects of Cl^- and HCO_3^- on the electrochemical behavior of 20CrMo steel and the interaction between them were investigated by the potential polarization, electrochemical impedance spectroscopy, and Mott-Schottky curve. In addition, the relationship between the $[Cl^-]/[HCO_3^-]$ ratio and the corrosion of 20CrMo Steel was studied.

2. EXPERIMENT

Specimens with dimensions of 10 mm×10 mm×2 mm were cut from a sheet of 20CrMo steel. All sides of the specimen surfaces were ground using a SiC emery paper down to 1000 gri. To prevent crevice corrosion, the samples were embedded in epoxy resin, leaving an area of 1 cm^2 exposed to solution prior to measurements. The exposed surface of the specimen was polished up to 1200 grit, cleaned in distilled water and degreased in methanol.

The base solution was 0.01 M Na_2SO_4 + 0.01 M Na_2CO_3. To examine the effects of Cl^- and HCO_3^- on the pitting of 20CrMo steel, NaCl and $NaHCO_3$ were added to the base solution to yield different Cl^- and HCO_3^- concentrations. All of the solutions were prepared from analytical-grade reagents and distilled water.

All the experiments were conducted using typical three-electrode electrochemical cells in the multi-ion solution. A saturated calomel electrode and a graphite rod was used as the reference and counter electrodes. The working electrodes were composed of 20CrMo steel.

First, the working electrode was immersed in a test solution for a certain time to reach a steady open-circuit potential. Next， polarization curves were obtained in a scanning potential range of -0.2 V to 2.0 V and at a scanning speed of 0.166 $mV \cdot s^{-1}$.

The impedance measurements were carried out in a frequency range of 10^5 Hz to 10^{-2} Hz, and the amplitude of the harmonic potential perturbation was 10mV. By the application of a stabilization potential of 0.5V for 60 min impedance plots were obtained.

Mott-Schottky measurements were carried out at a scanning potential was from -0.5 V to 1 V with a scanning rate of 40 mV/s.

3. RESULTS AND DISCUSSION

3.1 Potentiodynamic polarization curves for various HCO_3^- and Cl^- concentrations

Table 1 shows the pH values in different HCO_3^- concentration solutions. With the change in HCO_3^- concentration from 0.01 M to 0.1 M, the pH values decrease from 9.94 to 8.97. The magnitude of the pH value is affected by the hydrolysis reaction of HCO_3^- and CO_3^{2-}. The following element reactions, reactions (1)-(2), are possible. With the increase in the concentration of HCO_3^-, the hydrolysis of CO_3^{2-} decreases. On the contrary, the hydrolysis of HCO_3^- increases. Because the hydrolytic degree of CO_3^{2-} is greater than the hydrolytic degree of HCO_3^-, the content of OH^- reduces. And the pH value decreases.

$$CO_3^{2-} + H_2O \rightleftharpoons HCO_3^- + OH^- \quad (1)$$

$$HCO_3^- + H_2O \rightleftharpoons H_2CO_3 + OH^- \quad (2)$$

Fig.1 (a) shows the potentiodynamic polarization curves for 0.01-0.1 M solutions. In a 0.01 M $NHCO_3$ solution, active dissolution was observed on the 20CrMo steel surface. The HCO_3^- concentration of the solution is too low to form a passive film. The polarization curves exhibit a typical active-passive-transpassive characteristics [19] in 0.03-0.1 M $NaHCO_3$ solutions. A current peak and a small passive region in the 0.03 M $NaHCO_3$ solution are observed, suggesting that the surface iron matrix reacts with HCO_3^- to produce some iron compounds [20], these compounds are attached to the steel surface to form a short-lived and weak passive film. Two current peaks and a large steady passive region are observed in the 0.05 M $NaHCO_3$ solution. The second peak current is considerably greater than the first peak current. The previously generated corrosion products are transformed to other corrosion products, leading to the formation of a stable passivation film. There is no current peak is observed before the steady passive region in the 0.1 M $NaHCO_3$ solution. The pitting potentials increase rapidly with increasing HCO_3^- concentration in 0.03-0.1 M $NaHCO_3$ solutions.

With the change in HCO_3^- concentration from 0.01 M to 0.1 M, the pH values decrease. As the pH value decreases, more stable and protective Cr oxides are enriched in the film while Fe oxides gradually decompose [21], providing the film higher corrosion resistance and less conductivity. At high pH, chromium ions become more soluble, whereas iron oxides are more stable. When the pH value drops, the chromium concentration within the surface film increases due to the tendency for higher stability of the Cr oxides. Higher content of Cr oxides in the film layer provides corrosion-

resistant steel more excellent passivity at lower pH value [22].

The shape of the polarization curves in Fig.1 (b) significantly changes with the addition of Cl^-, indicating that the corrosion mechanism of 20CrMo steel changes. The $[Cl^-]/[HCO_3^-]$ ratio ranges from 0 to 2.5, the erosion of Cl^- sharply increases. The rate ranges from 2.5 to 5, the erosion of Cl^- increased slowly. The rate ranges from 5 to 10, and the erosion of Cl^- is basically stable. When the $[Cl^-]/[HCO_3^-]$ ratio is 10, a tiny anode peak is still existed which indicates that the passivation of HCO_3^- is slightly stronger than the erosion of Cl^-.

As shown in Fig.1 (c) a slight passive trend is still observed on the steel surface with a $[Cl^-]/[HCO_3^-]$ ratio of less than 20. At a ratio of greater than 33.3, active dissolution occurs at the surface. The threshold level of $[Cl^-]/[HCO_3^-]$ for the passivation of 20CrMo steel is between 20 and 33.3.

Table 2 summarizes the data of potentiodynamic polarization curves. With the increase in the concentration of HCO_3^- solution with or without Cl^-, the E_{corr} values increase, i_{corr} values gradually decrease and *Eb* values increase. It can be seen that for 20CrMo steel in alkaline solutions, less alkalinity offers better conditions for a higher protective passive film forming. This phenomenon probably accounts for the increasing enrichment of more protective Cr species in the passive film when the pH drops [21]. As the pH decreases, the film thickness increases [23].

The passivation is enhanced with increasing HCO_3^- concentration. With increasing Cl^- concentration, the E_{corr} values decrease, i_{corr} values increase and *Eb* values decrease. Cl^- increases the rate of corrosion of 20CrMo steel. It can accelerate the initiation of pitting.

Table 3 shows E_{corr} and i_{corr} values for different $[Cl^-]/[HCO_3^-]$ values. When the $[Cl^-]/[HCO_3^-]$ ratio ranges from 2.5 to 10, the E_{corr} values decrease rapidly in an exponential function, with easier corrosion. The rate ranges from 10 to 100, and the E_{corr} values are stable which shows that the erosion effect of Cl^- is basically equal. Fig.2 (a) shows that the relationship between E_{corr} and the $[Cl^-]/[HCO_3^-]$ rate can be described by the follow equation (3):

$$Y = -0.7196+0.4690\times0.6003^{x} \quad (3)$$

When the $[Cl^-]/[HCO_3^-]$ ratio ranges from 2.5 to 33.3, the i_{corr} values rapidly increase, indicating that the corrosion rate of 20CrMo steel increases. The ratio ranges from 33.3 to 100, and the i_{corr} values slowly increase. Fig.2 (b) shows the relationship between i_{corr} and the $[Cl^-]/[HCO_3^-]$ ratio. It is described by equation (4):

$$Y = 1.0528\times10^{-5}-4.37752\times10^{-6}\times097872^{x} \quad (4)$$

The effects of the $[Cl^-]/[HCO_3^-]$ ratio on E_{corr} and i_{corr} are not synchronous. The $[Cl^-]/[HCO_3^-]$ ratio ranges from 2.5 to 10, E_{corr} is more sensitive than i_{corr}. The $[Cl^-]/[HCO_3^-]$ ratio ranges from 2.5 to 100, i_{corr} is more sensitive than E_{corr}. Finally, the values of E_{corr} and i_{corr} are stable.

Table 1. The pH values of solutions

HCO_3^- concentration	0.01 M	0.03 M	0.05 M	0.1 M
pH value	9.94	9.53	9.30	8.97

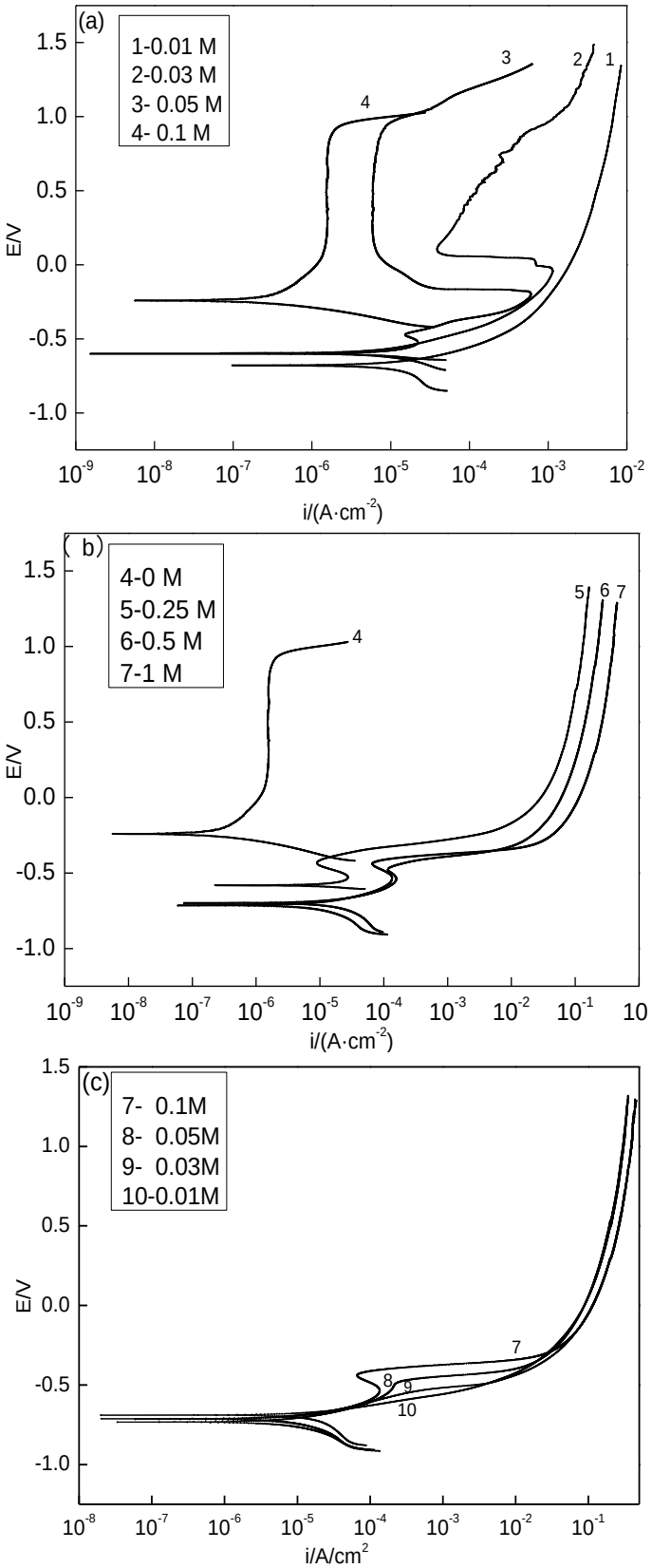

Figure 1. Potentiodynamic polarization curves for various HCO_3^- and Cl^- concentrations. (a) Different concentrations of $NaHCO_3$ (b) 0.1 M $NaHCO_3$, different concentrations of NaCl (c) 1 M NaCl, different concentrations of $NaHCO_3$

Table 2. Data of potentiodynamic polarization curves

Solution	E_{corr}/V	i_{corr}/(A·cm^{-2})	*Eb*/V
1	-0.6927	8.9572×10^{-6}	/
2	-0.6065	7.5008×10-6	0.1306
3	-0.6046	5.6465×10-6	0.8898
4	-0.2507	2.1704×10-7	0.8920
5	-0.5882	6.4339×10-6	-0.4231
6	-0.6830	6.7985×10-6	-0.4695
7	-0.7148	6.9883×10-6	-0.4344
8	-0.7189	7.4078×10^{-6}	/
9	-0.7196	8.7196×10^{-6}	/
10	-0.7203	1.0039×10^{-5}	/

Table 3. E_{corr} and i_{corr} values for different [Cl$^-$]/[HCO_3^-] values.

[Cl-]/[HCO3-]	2.5	5	10	20	33.3	100
E_{corr} values	1.0039×10^{-5}	8.7196×10^{-6}	8.7196×10^{-6}	6.9883×10^{-6}	6.7985×10^{-6}	6.4339×10^{-6}
i_{corr} values	-0.5882	-0.6830	-0.7148	-0.7189	-0.7196	-0.7203

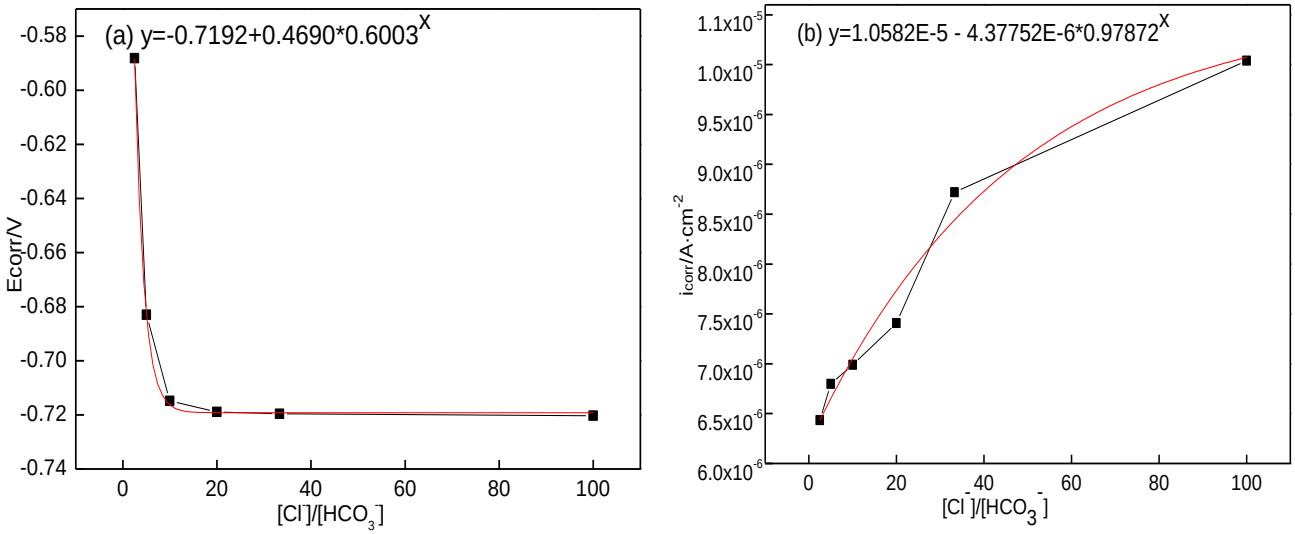

Figure 2. E_{corr} and i_{corr} values for different [Cl$^-$]/[HCO_3^-] values. (a) E_{corr} (b) i_{corr}

3.2 Electrochemical impedance spectroscopy behaviors

As seen in Fig.3, R1 represents the resistance of solution. R2 and CPE1 represent the resistance and capacity of the passivation film, respectively. R3 and C1 represent the resistance and capacity of the electrical double layer, respectively. The Warburg impedance exists in the electrochemical process.

Fig.3 (a) shows the Nyquist plots and equivalent circuits for different HCO_3^- concentrations. When HCO_3^- concentration is 0.03 M, there are one piece of capacitive impedance arc at high frequency and one piece of warbrug impedance at low frequency. The capacitive impedance arc

represents that the passivation film is complete. The warbrug impedance shows that the passive film is broken. The corrosion control system transforms from a charge control system to a diffusion control system. With the change in HCO_3^- concentration from 0.05 M to 0.1 M, there is a single capacitive impedance arc. With increasing the pH value, the radius of the capacitive impedance arc increases, and the passivation is stronger. The capacitance arc magnitude and overall impedance are even lager at pH 8.97, indicating the film formed at lower pH exhibits more protective behavior.

Table 4 summarizes the fitting data for the equivalent circuits. With the increase in the concentration of HCO_3^- solution from 0.03 M to 0.1 M, R1 values increase from 115.7 Ω•cm^2 to 754 Ω•cm^2, and R3 values gradually increase from 1.203×10^5 Ω•cm^2 to 1.603×10^7 Ω•cm^2. In addition, the CPE1 values decrease from 4.608×10^{-4} Ω^{-1}•cm^{-2}•S^{-n} to 3.489×10^{-6} Ω^{-1}•cm^{-2}•S^{-n}, and C1 values decrease 2.876×10^{-4} Ω^{-1}•cm^{-2}•S^{-n} to 3.798×10^{-6} Ω^{-1}•cm^{-2}•S^{-n}. With increasing HCO_3^- concentration, the resistance of the solution increases, and the movement of ions becomes more difficult. At a constant applied voltage, the current density of the passive film decreases, and the corrosion rate becomes slower.

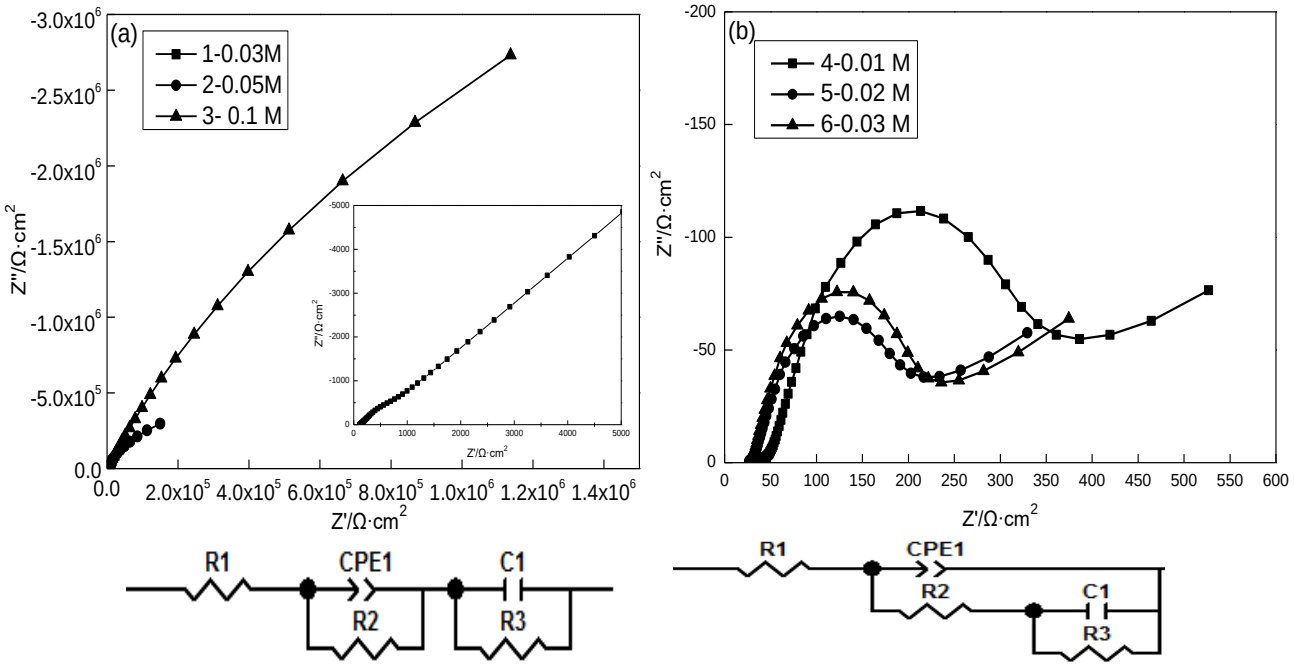

(a) different $NaHCO_3$ concentrations (b) 0.1 M $NaHCO_3$, different NaCl concentrations

Figure 3. The Nyquist plots and the equivalent circuits for different concentrations of $NaHCO_3$＋NaCl solutions

The concentration of NaCl solution changes from 0.01 M to 0.03 M in Fig.3 (b). A high-frequency capacitive impedance arc and low-frequency Warburg impedance are observed in all of the Nyquist plots. Warburg impedance exists for a wide range of Cl^- concentration, this implies that the corrosion processes are diffusion controlled whether in low or high chloride content solutions [24]. The radius of the semicircle gradually decreases, and the shape of the electrochemical impedance spectrum exhibits noticeable changes with increasing Cl^- concentration. Cl^- accumulates at the steel interface

which can cause the initiation and propagation of pits. After a pit is initiated, it grows both vertically and horizontally. After several minutes, a small hole is formed. The dissolution of metal in the initiation process produces anodic ions around the holes, resulting in the migration of chloride ions. The chloride ions diffuses in horizontal direction, leading to the final formation of a stable pit [25].

With increasing Cl^- solution concentration from 0.01M to 0.03M, R1 values decrease from 51.54 Ω•cm^2 to 31.16 Ω•cm^2, R2 values decrease from 137.1 Ω•cm^2 to 84.92 Ω•cm^2, R3 values decrease from 217.6 Ω•cm^2 to 128.2 Ω•cm^2. While CPE1 values increase from 9.388×10^{-3} Ω^{-1}•cm^{-2}•S^{-n} to 0.0144 Ω^{-1}•cm^{-2}•S^{-n}, C1 values increase from 7.256×10^{-3} Ω^{-1}•cm^{-2}•S^{-n} to 0.0134 Ω^{-1}•cm^{-2}•S^{-n}. With the addition of Cl^-, the corrosion mechanism of 20CrMo steel has changed. The passivation film exhibits a dynamic equilibrium state. With the presence of Cl^- in solution, the dynamic equilibrium of the passive film is destroyed, the dissolution rate of passive film is greater than the growth rate, and penetrating fracture occurs on the passive film. Cl^- not only destroys the passive film and leads to the occurrence of pitting corrosion, but also promotes the growth of pitting corrosion due to the concentration of Cl^- inside the pit [26].

Table 4. Values of equivalent circuits

Solution	R_1 Ω•cm^2	R_2 Ω•cm^2	C_1 Ω^{-1}•cm^{-2}•S^{-n}	R_3 Ω•cm^2	CPE_1 Ω^{-1}•cm^{-2}•S^{-n}	n
1	115.7	166.3	2.876×10^{-4}	1.203×10^{5}	4.608×10^{-4}	0.515
2	151.4	83.04	1.226×10^{-5}	1.228×10^{6}	3.070×10^{-5}	0.874
3	754	26.45	3.798×10^{-6}	1.603×10^{7}	3.489×10^{-6}	0.864
4	51.54	137.1	7.256×10^{-3}	217.6	9.388×10^{-3}	0.481
5	32.93	84.49	-0.4231	144.2	0.0132	0.519
6	31.16	84.92	-0.4695	128.2	0.0144	0.514

3.3 Semiconducting nature of the passive film

A linear relationship between capacitance and the applied potential can be expressed by the Mott–Schottky equation .

$$C^{-2} = \frac{2}{\varepsilon\varepsilon_0 e N_D}\left(E - E_{FB} - \frac{kT}{e}\right) \qquad \text{n-type semiconductor}$$

$$C^{-2} = -\frac{2}{\varepsilon\varepsilon_0 e N_A}\left(E - E_{FB} - \frac{kT}{e}\right) \qquad \text{p-type semiconductor}$$

Where ε is the dielectric constant of the passive film, ε_0 is the permittivity of free space (8.854×10^{-14} F/cm), e is the electron charge (1.602×10^{-19}C), N_D and N_A are the donor and acceptor densities. E_{FB} is the flat-band potential, T is the absolute temperature (298K), and k is the Boltzmann constant (1.38×10^{-23}J/K). The dielectric constant of the passive film on the stainless steels is 15.6 [27]. N_D and N_A can be determined from the slope of the experimental C^{-2} vs. applied potential.

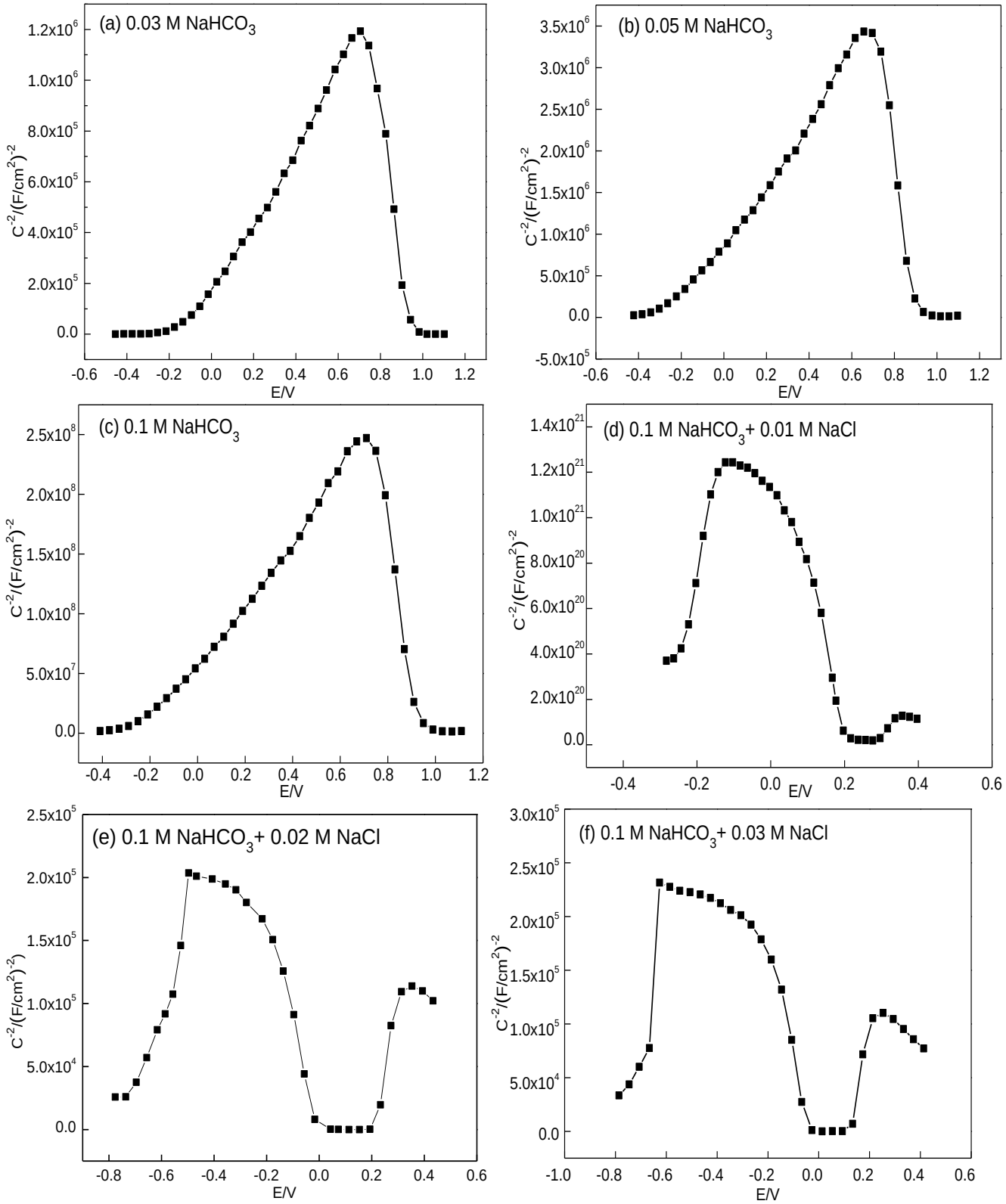

Figure 4. The Mott-Schottky plots for different concentrations $NaHCO_3$ and NaCl solutions

Fig.4 shows the Mott–Schottky plots at different concentrations of $NaHCO_3$ and NaCl solutions. Two lines with positive and negative slopes, respectively, characterized by different capacitance

behaviors and separated by peak potentials in all the Mott–Schottky plots, are observed. With the increase in the scanning potential, the presence of a peak region is observed, relates to the excess charge present on the oxide surface. The positive region of the straight line is indicative of the n-type semiconducting behavior (iron oxide), while the negative potential region of the straight line indicates the p-type semiconducting behavior (chromium oxide) of the passive film [28].

With the increase in the $NaHCO_3$ solution concentration changes from 0.03 M to 0.05 M and 0.1 M, the peak potentials are 0.70V, 0.69V, and 0.71V, respectively. The N_D and N_A values decrease with increasing HCO_3^- concentration. Lower values are observed in the alloy with the highest HCO_3^- concentration. The donors or acceptors in the semiconducting passivation film constitute defects, e.g., cation and anion vacancies. The concentration of electronic defects decreases with pH and that the films formed at highest pH present the highest density of donors, indicating a more conductive behavior. Generally, the rupture of the metal passivation film and the initiation of the pitting generally occur at the defective locations within the passivation film. The internal structure in the passivation film is more stable with few defects [29].

With the increase in the NaCl solution concentration changes from 0.03 M to 0.05 M and 0.1 M, the peak potentials are 0.70V, 0.69V, and 0.71V, respectively. With the increase in the Cl^- concentration, the peak potential become more negative. The Cl^- from the solution is adsorbed on the passivation film surface, hence, the concentration of negative charge on the surface increases. With increasing Cl^- concentration, the N_D and N_A values increase and defects increase.

4. CONCLUSION

(1)With the increase in the HCO_3^- concentration in the simulated oil field environment, the .resistance to pitting corrosion and transpassive potential of 20CrMo steel increased. The resistance to pitting corrosion and transpassive potential decreased with increasing Cl^- concentration. Cl^- can decrease the pitting potential and improve the dissolution rate of the passivation film.

(2)The HCO_3^- and Cl^- concentrations affect the semiconducting nature of the passive film. Capacitance studies revealed the existence of n-and p-type semiconductors. The N_D and N_A values decreased with increasing HCO_3^- concentration. The opposite side, the N_D and N_A values, increased with increasing Cl^- concentration. These results indicated that the oxide layers of the passive film are modified by HCO_3^- and Cl^-.

(3)The ratio of $[Cl^-]/[HCO_3^-]$ in the multi-ion mixed system is closely related to the corrosion of 20CrMo steel. When the $[Cl^-]/[HCO_3^-]$ ratio is less than 20, the passivation of HCO_3^- is dominant. On the contrary, when the $[Cl^-]/[HCO_3^-]$ ratio is greater than 20, the active dissolution of 20CrMo steel occurs. The $[Cl^-]/[HCO_3^-]$ ratio ranged from 0.1 to 0.2, and the erosion of Cl^- in the passivation film increases rapidly. The $[Cl^-]/[HCO_3^-]$ ratio ranged from 0.2 to 0.3, and the erosion of Cl^- slowly increased.

References

1. M.C. Li, Y.F Cheng, *Electrochim. Acta.*, 53(2008)2831.

2. C.W. Du, X.G. Li, X. Chen, *Acta Metall. Sin.*, 21(2008)235.
3. D.G. Li, Y.R. Feng, Z.Q. Bai, *Appl. Surf. Sci.*, 254(2008)2837.
4. J.G. Gonzalez-Rodriguez, M.G. Casales, V.M. Salinas-Bravo, *Corrosion (Houston, Tx, U.S.).*, 58(2002)584.
5. Z. Lu, C. Huang, D. Huang, *Corros. Sci.*, 48(2006)3049.
6. L. Hamadou, A. Kadri, N. Benbrahim, *Appl. Surf. Sci.*, 252(2005)1510.
7. D.G. Li, Y.R. Feng, Z.Q. Bai, *Electrochim. Acta.*, 52(2007)7877.
8. P. Marcus, V. Maurice, H.H. Strehblow, *Corros. Sci.*, 50(2008)2698.
9. Y.F. Cheng, M. Wilmott, J.L.Luo, *Appl. Surf. Sci.*, 152(1999)161.
10. S.M.A.E. Haleem, S.A.E. Wanees, A. Bahgat, *Corros. Sci.*, 75(2013)1.
11. S.M.A.E. Haleem, S.A.E. Wanees, E.E.A.E. Aal, *Corros. Sci.*, 52(2010)1675.
12. Z.H. Dong, S. Wei, A.Z. Guo, *Electrochim. Acta.*, 56(2011)5890.
13. M. Liu, X. Cheng, X. Li, *Constr. Build. Mater.*, 93(2015)884.
14. Y. Zuo, H. Wang, J. Zhao, *Corros. Sci.*, 44(2002)13.
15. Y. Zuo, H. Wang, J. Xiong, *Corros. Sci.*, 44(2002)25.
16. G.F. Qiao, J.P. Ou, *Electrochim. Acta.*, 52(2007)8008.
17. K.Y. Ann, H.W. Song, *Corros. Sci.*, 49(2007)4113.
18. V.T. Ngala, C.L. Paga, M.M. Paga, *Mater. Corros.*, 55(2004)511.
19. Z. Lu, C. Huang, D. Huang, *Corros. Sci.*, 48(2006)3049.
20. J.M. Blengino, M. Keddam, J.P. Labbe, *Cheminform.*, 26(1995)621.
21. L. Freire, M.J. Carmezim, M.G.S. Ferreira, *Electrochim Acta*., 55(2010)6174.
22. Z.Y. Ai, J.Y. Jiang, W. Sun, *Appl Surf. Sci.*, 389(2016)1126.
23. C.O.A. Olsson, D. Landolt, *Electrochim Acta.*, 48(2003)1093.
24. Y.F. Wang, G.G. Cheng, *Appl. Surf. Sci.*, 349(2015) 746.
25. Y.F. Wang, G.G. Cheng, Y. Li, *Corros. Sci*., 111(2016) 508.
26. L.B. Niu, K. Nakada, *Corros Sci.*, 96(2015)171.
27. C.A. Gervasi, M.E. Folquer, A.E. Vallejo, *Electrochim. Acta.*, 50(2005)1113.
28. S. Fujimoto, H. Tsuchiya, *Corros. Sci.*, 49(2007)195.
29. S. Ningshen, U.K. Mudali, V.K. Mittal, *Corros. Sci.*, 49(2007)481.